Preliminary Study of Multichain-based Loran Positioning Accuracy for a Dynamic User in South Korea

Pyo-Woong Son[1], Joon Hyo Rhee[1], Younghoon Han[2], Kiyeol Seo[2], Jiwon Seo[1]

[1]School of Integrated Technology
Yonsei University
Incheon, Republic of Korea

[2]Marine Safety and Environmental Research Department
Korea Research Institute of Ships and Ocean Engineering
Daejeon, Republic of Korea

***Abstract*—The long range navigation (Loran) system is a terrestrial high-power radionavigation system using 100-kHz signals. It can be a complementary positioning, navigation, and timing (PNT) system for maritime users because of its robustness to radio frequency interference, even though its positioning accuracy is low compared to that of GNSS. South Korea has suffered from GPS jamming attacks from the North and decided to deploy a nationwide enhanced Loran (eLoran) system. However, the Korean eLoran project has been delayed several times because of contractual problems and other issues. Therefore, we developed a multichain-based Loran positioning method to improve the current Loran positioning performance, which does not require hardware upgrades of existing Loran transmitters to eLoran capability. We have previously demonstrated an approximately 15-m (95%) accuracy for a static user by applying our multichain-based Loran positioning algorithm and the time-difference-of-arrival (TDOA)-based temporal additional secondary factor (ASF) correction method when a user was approximately 12 km from a differential correction station. In this study, we examine the improved Loran positioning performance for a dynamic user based on the multichain algorithm and the existing Loran infrastructure in Northeast Asia. TDOA-based ASF maps, which are different from conventional time-of-arrival (TOA)-based ASF maps for eLoran, are generated to compensate for spatial ASF errors for the dynamic user.**

Keywords—Loran; multichain-baseed positioning; accuracy; ASF map

I. INTRODUCTION

Global navigation satellite systems (GNSS) are widely used and have become the primary source for navigation. However, GNSS are vulnerable to radio frequency interference (RFI) because of their weak signal strength [1]-[6]. In addition, the performance of GNSS is affected by anomalous ionospheric conditions due to severe space weather [7]-[12]. Although various anti-interference techniques [13]-[19] have been developed to mitigate the impact of RFI to GNSS, their effectiveness is limited under a high-power RFI.

The long range navigation (Loran) system is based on high-power radio signals transmitted from transmitters located at known locations on land [20]. A user position is calculated by hyperbolic navigation using the time-difference-of-arrival (TDOA) values of the received Loran signals. Because its signal power is significantly greater than that of GNSS, Loran does not have the same weakness that GNSS have, although the navigation performance of Loran is not as good as that of GNSS. Thus, integrated GPS/Loran receivers can provide a more resilient navigation solution [21]–[23]. Loran signals can also be used for various applications such as location-based services and geo-security [24]–[26].

North Korea has attempted several GPS jamming attacks on South Korea in recent years, and numerous South Korean ships have been impacted because they rely on GPS for navigation. To provide resilient position, navigation, and timing (PNT) information to maritime users, South Korea proposed to deploy a nationwide eLoran system in 2013 [27]. However, the South Korean eLoran project has been delayed and revised several times because of contractual problems and other issues. Therefore, we have developed a multichain-based Loran positioning algorithm [28] to improve the current Loran positioning performance, which can be operated by the existing Loran transmitters without requiring any hardware upgrades to reach eLoran capability. The conventional Loran system employs a TDOA-based positioning algorithm because Loran transmitters are time-synchronized only within the same Loran chain [29]. Thus, the TDOA measurement cannot be generated from the signals of different chains. Our multichain-based Loran positioning algorithm resolves this limitation.

In the previous study, we have demonstrated the performance of the multichain algorithm in a static environment [28]. The positioning performance of a static user showed 15-m (95%) accuracy during a 21-hour campaign with spatial additional secondary factor (ASF) compensation and temporal ASF correction. Because the user was stationary, spatial ASF was compensated for by a single spatial ASF value instead of spatial ASF maps. The temporal ASF correction messages were generated by a differential correction station, also known as DLoran station.

In the current study, we demonstrate the performance of the multichain algorithm in a dynamic environment. To evaluate the performance of the algorithm in a dynamic environment, a GPS/Loran integrated receiver mounted on a ground vehicle was used to collect signals while the vehicle traveled at a speed

978-1-5386-1647-5/18/$31.00 ©2018 IEEE

of 30–60 km/h in a 4.5 km route. For the dynamic test, TDOA-based spatial ASF maps were generated along the route.

Section II explains TDOA-based temporal ASF correction generation by a DLoran station. TDOA-based spatial ASF map generation for the dynamic test is discussed in Section III. After presenting the dynamic test rests in Section IV, the conclusion is given in Section V.

II. TDOA-BASED TEMPORAL ASF CORRECTION

The Loran signal propagates along a path and is delayed by various factors. The delay error can be divided into three major categories: the primary factor (PF), which is the delay produced by the atmosphere; the delay factor that occurs as the signal passes over the sea, which is called the secondary factor (SF); and the delay factor that occurs as it passes over the land, which is called the ASF. The ASF is divided into spatial and temporal ASF, and each ASF must be compensated to improve Loran positioning accuracy. The PF and SF are easily compensated by Brunavs' equation [30].

The ASF is calculated as the difference between the theoretical propagation time of the signal based on the distance from each transmitter to a user and the actual propagation time, after the PF and SF compensation, measured by the user. Because the DLoran station knows its exact surveyed location, the theoretical propagation time between the DLoran station and Loran transmitters can be calculated. However, unlike eLoran, actual propagation time is hard to obtain because TOA measurements are not available in Loran. Instead, TDOA measurements are utilized in Loran, and so the ASF within TDOA measurements need to be compensated. Thus, TDOA-based ASF corrections [28] are necessary for Loran, which are different from conventional TOA-based ASF corrections for eLoran.

The TDOA-based ASF is the difference between the measured TDOA value and the geometric TDOA value after the PF and SF compensation. Fig. 1 shows example TDOA measurements between the Gwangju and Pohang transmitters with PF, SF, spatial ASF, and temporal ASF components indicated.

We established a DLoran station at Yonsei University, Incheon, Korea. In addition, an H-field antenna and eLoran/GPS integrated receiver (LORADD-M), produced by reelektronika, was installed on the rooftop of the building as in Fig. 2. Temporal ASF corrections were generated by the DLoran station, and an example of temporal ASF corrections are shown in Fig. 3.

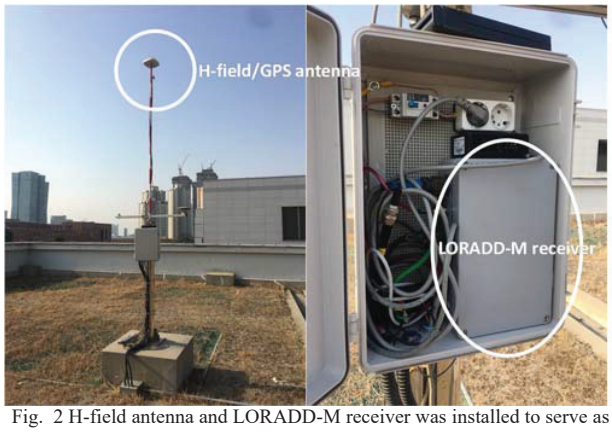

Fig. 2 H-field antenna and LORADD-M receiver was installed to serve as a DLoran station.

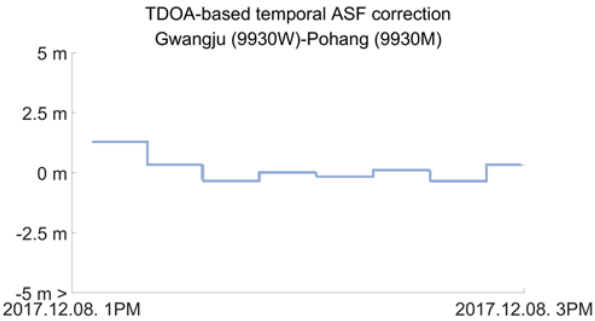

Fig. 3 Temporal ASF corrections. Five-minute averaging time and 15-min update interval were used.

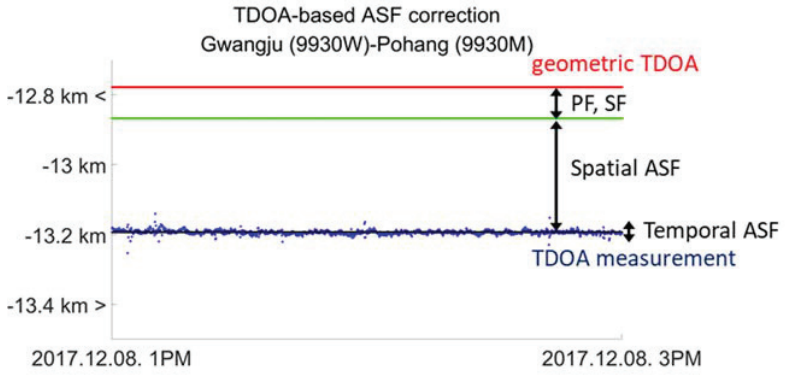

Fig. 1 TDOA measurements between Gwangju and Pohang transmitters. TDOA measurements (blue) contain PF, SF, spatial ASF, and temporal ASF components.

III. TDOA-based Spatial ASF Map Generation

For the ASF compensation, required to improve the positioning performance of Loran, a DLoran station that can generate the temporal ASF corrections and ASF maps, which compensate for the spatial ASF, are both required [31]. The ASF maps are produced based on spatial ASF measurements in the service area [32]. First, a DLoran station generates temporal ASF corrections. Then, an ASF survey receiver obtains the spatial ASF components by excluding the temporal ASF corrections from the measured ASF values. The survey area is divided into a grid of regular intervals, usually 500 m, and a representative spatial ASF value is set for each grid point using an interpolation technique. With an extrapolation technique, ASF maps can be expanded to a nearby non-survey area.

To survey the spatial ASF values, we installed a GPS/eLoran integrated receiver (LORADD-SP), manufactured by reelektronika, on a car, as shown in Fig. 4. The temporal ASF corrections were applied to obtain the spatial ASF values by post-processing. For the ASF map generation, the car drove three round-trips along an approximately 4.5 km road in Sejong, Korea. ASF maps were generated with 9 grids along the latitude and 16 grids along the longitude, and the size of each grid was approximately 200 m. This 200 m grid size is smaller than the regular 500 m grid size for sea, because we expect that the variation of spatial ASF values on land would be larger than at sea. A separate ASF map needs to be generated for each TDOA pair. Because nine Loran signals from seven transmitters were available in the region where the experiment was performed, ${}_9C_2 = 36$ pairs of TDOA-based ASF maps were generated (two transmitters are dual-rated). Fig. 5 is an example TDOA-based ASF map between the signals of the Gwangju and Pohang transmitters.

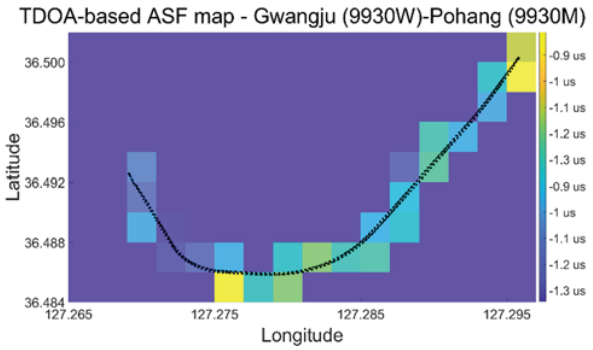

Fig. 5 TDOA-based ASF map between Gwangju and Pohang transmitters. The black points represent the GPS trajectory of the ASF survey vehicle.

IV. Positioning Accuracy of a Dynamic User in Sejong, Korea

To evaluate the dynamic performance of the multichain-based positioning algorithm [28], an experiment was conducted along the same route where the ASF survey was performed. The vehicle traveled at a speed of approximately 40–60 km/h. Although nine Loran signals were available in the region, only seven signals from five transmitters (i.e., 9930M from Pohang; 9930W from Gwangju; 7430M and 8390Y from Rongcheng; 7430X and 8390M from Xuancheng; and 7430Y from Helong) were of good-enough quality for use in positioning.

If we apply the conventional Loran positioning algorithm, only signals from the same chain can be utilized for positioning. Thus, 7430M, 7430X, and 7430Y signals were used for conventional Loran positioning, and its positioning accuracy was 87 m (95%).

This performance can be enhanced if we apply the multichain-based Loran positioning algorithm [28] that can utilize all received Loran signals regardless of their chains. The block points in Fig. 6 represent the GPS positions of the vehicle, thus showing the trajectory of the vehicle. The red

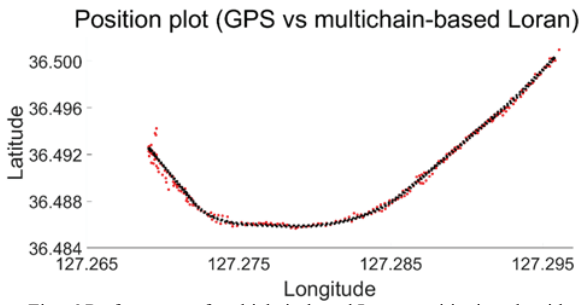

Fig. 6 Performance of multichain-based Loran positioning algorithm during a dynamic test. The red points are derived from Loran; the black points are derived from GPS.

Fig. 4 GPS/Loran equipment for the ASF survey.

points are the positions obtained using the multichain algorithm, with a positioning accuracy of 39 m (95%). This is a significant improvement over the 87 m accuracy of the conventional algorithm.

V. Conclusion

This study showed the feasibility of multichain-based Loran positioning in a dynamic environment. With the existing Loran signals in Northeast Asia, we tested its positioning performance in the dynamic environment. A DLoran station capable of generating TDOA-based temporal ASF corrections was installed. TDOA-based ASF maps were generated by ASF survey to correct the spatial ASF of a dynamic user. The positioning result of the multichain algorithm was compared to that of a conventional algorithm; the multichain positioning accuracy was 39 m (95%) with 100% position availability. In fact, the signal-to-noise ratios (SNRs) of the received Loran signals during this experiment on land were low. Because higher SNRs are expected at sea, the positioning accuracy of a ship is expected to be better than that obtained in this study.

Acknowledgment

This research was a part of the project titled “Development of enhanced Loran system,” funded by the Ministry of Oceans and Fisheries, Korea. This research was also supported by the Ministry of Science and ICT (MSIT), Korea, under the “ICT Consilience Creative Program” (IITP-2018-2017-0-01015) supervised by the Institute for Information & Communications Technology Promotion (IITP).

References

[1] F. D. Nunes and F. M. G. Sousa, “GNSS blind interference detection based on fourth-order autocumulants,” *IEEE Transactions on Aerospace and Electronic Systems*, vol. 52, no. 5, pp. 2574–2586, 2016.

[2] M. Wildemeersch, C. H. Slump, and A. Rabbachin, “Acquisition of GNSS signals in urban interference environment,” *IEEE Transactions on Aerospace and Electronic Systems*, vol. 50, no. 2, pp. 1078–1091, 2014.

[3] E. Axell, F. M. Eklöf, P. Johansson, M. Alexandersson, and D. M. Akos, “Jamming detection in GNSS receivers: performance evaluation of field trials,” *Navigation*, vol. 62, no. 1, pp. 73–82, 2015.

[4] E. Kim and J. Seo, “SFOL pulse: a high accuracy DME pulse for alternative aircraft position and navigation,” *Sensors*, vol. 17, no. 10, art. no. 2183, 2017.

[5] B. Motella and L. L. Presti, “Methods of goodness of fit for GNSS interference detection,” *IEEE Transactions on Aerospace and Electronic Systems*, vol. 50, no. 3, pp. 1690–1700, 2014.

[6] M. Abdizadeh, J. T. Curran, and G. Lachapelle, “New decision variables for GNSS acquisition in the presence of CW interference,” *IEEE Transactions on Aerospace and Electronic Systems*, vol. 50, no. 4, pp. 2794–2806, 2014.

[7] A. Coster and A. Komjathy, “Space weather and the Global Positioning System,” *Space Weather*, vol. 6, no. 6, pp. S06D04, 2008.

[8] J. Seo, T. Walter, and P. Enge, “Availability impact on GPS aviation due to strong ionospheric scintillation,” *IEEE Transactions on Aerospace and Electronic Systems*, vol. 47, no. 3, pp. 1963–1973, 2011.

[9] J. Seo and T. Walter, “Future dual-frequency GPS navigation system for intelligent air transportation under strong ionospheric scintillation,” *IEEE Transactions on Intelligent Transpportation Systems*, vol. 15, no. 5, pp. 2224–2236, 2014.

[10] Y. Jiao and Y. T. Morton, “Comparison of the effect of high-latitude and equatorial ionospheric scintillation on GPS signals during the maximum of solar cycle 24,” *Radio Science*, vol. 50, no. 9, pp. 886–903, 2015.

[11] J. Lee, Y. T. Morton, J. Lee, H.-S. Moon, and J. Seo, “Monitoring and mitigation of ionospheric anomalies for GNSS-based safety critical systems,” *IEEE Signal Processing Magazine*, vol. 34, no. 5, pp. 96-110, 2017.

[12] J. Seo, T. Walter, T.-Y. Chiou, and P. Enge, “Characteristics of deep GPS signal fading due to ionospheric scintillation for aviation receiver design,” *Radio Science*, vol. 44. art. no. RS0A16, 2009.

[13] R. L. Fante, J. J. Vaccaro, "Wideband cancellation of interference in a GPS receive array," *IEEE Transactions on Aerospace and Electronic Systems*, vol. 36, no. 2, pp. 549-564, 2000.

[14] Y.-H. Chen, J. C. Juang, D. S. De Lorenzo, J. Seo, S. Lo, P. Enge, D. M. Akos, “Real-time software receiver for GPS controlled reception pattern antenna array processing”, in Proc. ION GNSS, Portland, OR, USA, 2010, pp. 1932–1941.

[15] D. S. De Lorenzo, S. C. Lo, J. Seo, Y.-H. Chen, P. K. Enge, “The WAAS/L5 signal for robust time transfer: Adaptive beamsteering antennas for satellite time synchronization,” in Proc. ION GNSS, Portland, OR, USA, 2010, pp. 2106–2116.

[16] Y.-H. Chen, J. C. Juang, D. S. De Lorenzo, J. Seo, S. Lo, P. Enge, D. M. Akos, “Real-time dual-frequency (L1/L5) GPS/WAAS software receiver,” in Proc. ION GNSS, Portland, OR, USA, 2011, pp. 767–774.

[17] J. Seo, Y.-H. Chen, D. S. De Lorenzo, S. Lo, P. Enge, D. Akos, and J. Lee, “A real-time capable software-defined receiver using GPU for adaptive anti-jam GPS sensors,” *Sensors*, vol. 11, no. 12, pp. 8966–8991, 2011.

[18] Y.-H. Chen, J. C. Juang, J. Seo, S. Lo, D. M. Akos, D. S. De Lorenzo, and P. Enge, “Design and implementation of real-time software radio for anti-interference GPS/WAAS sensors,” *Sensors*, vol. 12, no. 12, pp. 13417–13440, 2012.

[19] K. Park, D. Lee, and J. Seo, “Dual-polarized GPS antenna array algorithm to adaptively mitigate a large number of interference signals,” *Aerospace Science and Technology*, doi:10.1016/j.ast.2018.04.029, in press.

[20] P. Enge, E. Swanson, R. Mullin, K. Ganther, A. Bommarito, and R. Kelly, “Terrestrial Radionavigation Technologies,” *Navigation*, vol. 42, no. 1, pp. 61–108, 1995.

[21] G. L. Roth and P. W. Schick, “New Loran capabilities enhance performance of hybridized GPS/Loran receivers,” *Navigation*, vol. 46, no. 4, pp. 249–260, 1999.

[22] A. J. Fisher, “Loran-C cycle identification in hard-limiting receivers,” *IEEE Transactions on Aerospace and Electronic Systems*, vol. 36, no. 1, pp. 290–297, 2000.

[23] A. Grant, P. Williams, N. Ward, and S. Basker, “GPS jamming and the impact on maritime navigation,” *Journal of Navigation*, vol. 62, no. 2, pp. 173–187, 2009.

[24] D. Qiu, “Security from Loran,” Ph.D. dissertation, Stanford University, Stanford, CA, USA, 2009.

[25] D. Qiu, D. Boneh, S. Lo, and P. Enge, “Reliable location-based services from radio navigation systems,” *Sensors*, vol. 10, no. 12, pp. 11369–11389, 2010.

[26] D. Qiu, S. Lo, P. Enge, and D. Boneh, “Pattern classification for geotag generation,” in Proc. ION GNSS, Savannah, GA, USA, 2009, pp. 1819–1827.

[27] J. Seo and M. Kim, “eLoran in Korea–current status and future plans,” in Proc. European Navigation Conference, Vienna, Austria, 2013.

[28] P.-W. Son, J. H. Rhee, and J. Seo, “Novel multichain-based Loran positioning algorithm for resilient navigation,” *IEEE Transactions on Aerospace and Electronic Systemsm*, vol. 54, no. 2, pp. 666-679, 2018.

[29] S. Lo, B. Peterson, P. Enge, and P. Swaszek, “Loran data modulation: extensions and examples,” *IEEE Transactions on Aerospace and Electronic Systems*, vol. 43, no. 2, pp. 628–644, 2007.

[30] RTCM SC-127, Minimum performacne standards for marine eLoran receiving equipment, 2017.

[31] C. Hargreaves, P. Williams, and M. Bransby, “ASF quality assurance for eLoran,” in Proc. IEEE/ION PLANS, Myrtle Beach, SC, USA, 2012, pp. 1169–1174.

[32] P. Williams and D. Last, “Mapping the ASFs of the Northwest European Loran-C system,” *Journal of Navigation*, vol. 53, no. 2, pp. 225–235, 2000.